Multimodal Biometrics Authentication Using Thermal Hand Vein and Hand Dorsa

Kannu Priya
PG Scholar, *Department of Computer Science and Engineering , CMR Institute of Technology*, Bengaluru,India, kannu.tcs@gmail.com

Dr. R. Kesavamoorthy
Associate Professor, *Department of Computer Science and Engineering , CMR Institute of Technology*, Bengaluru,India, kesavamoorthy.r@cmrit.ac.in

Dr. Raja M.
Professor, Department of Computer Science and Engineering, CMR Institute of Technology, Bengaluru, India, raja.m@cmrit.ac.in

Dr.S.P.Anandaraj
Associate Professor Selection Grade, Department of Computer Science and Engineering, Presidency University, Bangalore, India, anandsofttech@gmail.com

Dr. D. Loganathan
Professor, Department of Computer Science and Engineering, HKBK College of Engineering, Bangalore, India, dloganathan.cs@hkbk.edu.in

Dr. Thanga Mariappan L.
Associate Professor, Computer Science and Engineering, School of Computing, Vel Tech Rangarajan Dr Sagunthala Institute of Science and Technology, Chennai, India, thangamariappanme@gmail.com

Abstract:

The dorsal part of the hand's dorsal veins, which are internal thermal veins beneath the skin, and the hand's outward appearance/texture, also known as the hand appearance, are combined in this work to create a revolutionary personal authentication mechanism. Using a digital camera and an infrared thermal camera, respectively, it is possible to concurrently acquire photos of the hand-vein and the hand's appearance. By fusing the above features based on the fusion at score-level and applying integration rules, a claimed identity can be verified. Each module we are individually assessed in terms of Error rate prior to the fusion, and individual weights are assigned based on performance. The multimodal system has a 98% accuracy rate according to the experimental data, which makes it an effective security solution.

Keywords: Biometrics, Thermal Hand Vein, Hand Dorsa, Multimodal security system

DOI Number: 10.14704/nq.2022.20.9.NQ44392 **Neuro Quantology 2022; 20(9):3423-3432**

I. Introduction

Many authentication systems have been created employing fingerprint [1]-[3], palmprint [4]-[6] and hand-geometry [7]-[8] with high user acceptance. Biometrics based on hand, specifically palm portion, is explored intensively in recent years. However, because the human body's outermost region is where people unintentionally level their fingerprints and palm prints, this kind of carelessness exposes these modes of transportation to security dangers.

The available unimodal biometric systems are prone to imposter attacks. The overall errors in the system are also a concern for designing a system for a larger population like India. The available multimodal biometric systems are generally less prone to imposter attack and more accurate than unimodal systems. However, multimodal biometric systems are generally cost ineffective and less user convenient due to multiple sensor involvement. The literature review shows us that mostly all available multimodal biometrics systems are static and based on a fixed decision threshold for accept/reject decisions. Due to its resistance to impostor assaults, vein patterns are steadily gaining recognition as a promising biometric feature for personal authentication. It typically grows as the body does starting in childhood and is pretty steady from the age of 16 to 60. People in this age range have vein patterns that can be used as a distinctive biometric. Vein patterns, which are found below the skin, are a more secure biometric characteristic because they can't be faked by an imposter attack. However, it's a concealed component of the human being & it's extremely sensitive at factors outside of our body, such as humidity and temperature [9]. Therefore, it is necessary to create a bimodal system that may incorporate vein patterns with other biometric characteristics. The dorsal portion of the hand's texture and shape—referred to as hand appearance in this chapter—are used as biometric traits. This work's primary goal is to create a system employing the patterns present in vein of palm dorsa & its shape taken from hand's dorsal region. Images of the hand vein patterns are obtained using an infrared thermal camera, whereas pictures of the hand shapes are obtained using a visible light camera. Before making the final accept/reject decision, both biometric features can be concurrently derived from the claimed identity and combined. This bimodal system's goals are to I improve each user's performance of their hand vein and hand appearance by fusing them together, and (ii) fend off imposter attacks anytime they are used for personal verification Prior Work

Bimodal/multimodal systems have a history dating back more than ten years, during which time numerous advancements have been made. In 1998, Hong et al. [10] suggested a bimodal method utilizing both the fingerprint and the face. Taking images of the face and lip movement taken from the same video clip, Frischholz et al. [11] revealed what is likely the first commercially available BioID system. They used their approach to attain an equal error rate (EER) of less than 1%. Fierrez et al[12]'s creation of a multimodal biometric system combines.

A bimodal system made up of the hand-geometry and palmprint biometric modalities were developed by Kumar et al. [13]. One type of fusion was done at the feature level & another one was taken on the score level. Their bimodal approach produces a score-level fusion FAR of 0% at FRR of 1.41%. It has been demonstrated that the sum rule results in a FAR of 0.03percentage points at a FRR of 1.78percentage points whereas the fingerprint results in a FAR of 0.01% at a FRR of 25%. Another multimodal framework using hand-geometry, fingerprint, and face biometrics has been proposed by Jain et al. [15].

A. *Motivation*

There are very few efforts on making a bimodal system employing hand vein patterns. The literature has shown various promising efforts on unimodal hand-vein/palm-vein or hand shape/hand-geometry [16]-[18]. The work on finger vein by Kumar et al. [16] is also merits a mention in this direction. However, in the literature, there has not been any effort on making the infrared thermal vein patterns and hand appearance from the same dorsal part of the hand.

B. *Our Work*

By combining vein of hand traits with the appearance of hand & modalities at the score-level, as shown in Fig. 1, a bimodal system was created. For these objectives, vein patterns are acquired using an infrared thermal camera, while the look of user's hands are captured using a standard digital camera. The Radon transform captures

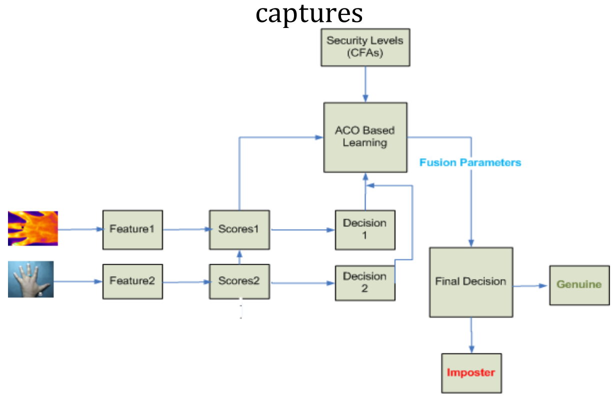

Fig. 1. Flow chart of bimodal adaptive system

textural patterns Here, characteristics from the hand-vein patterns are retrieved by combining the intensities along all lines that could possibly exist in the image [19]. We fused the modalities of hand appearance & vein trends at the score level, as depicted in Fig.1, a bimodal system was created. For these objectives, vein patterns are acquired using an infrared thermal camera, while the look of the hands is captured using a standard digital camera.

Most of the prior work on multimodal systems, biometrics traits are acquired from different sensors which not only increases overall cost but also user inconveniences. A hand Infrared thermal vein based unimodal authentication system hand dorsa (Shape + Appearance) based unimodal authentication system. An adaptive multimodal biometrics framework using hand vein and hand dorsa which can dynamically choose a decision threshold based on an application. We use image processing, pattern recognition, and evolutionary technique based optimization for implementing the adaptive multimodal biometrics framework.

The paper has been arranged in the following way: In *Division I*, image acquisition and the normalization of both the hand vein and hand appearance modalities are provided, in *Division II* their feature extraction methods are given, in *Division III*, experimental results and a discussion are presented. Finally, the conclusion is depicted in *Division IV*.

I. Image Acquisition and Normalization

A. Hand Vein Acquisition and Normalization

On the dorsal portion of the hand, the vein patterns found beneath the skin are not visible in normal lighting, and the skin's hair, moles, warts, etc. prevent an accurate image capture by a standard digital camera. Additional colours and characteristics of fat/thick skins make people less visible. According to the weather, the inside temperature is set between 100°C and 300°C, and the relative humidity is set between 25 and 50 percent. In outdoor settings, thermal imaging vision is compromised, making it exceedingly challenging to distinguish venous patterns from background [21]. When a user enters an indoor location for imaging after leaving an outdoor setting, the temperature can change suddenly, affecting visibility even when the photos are acquired indoors. To combat the aforementioned problem, we pause the acquisition process for a brief period of time until the operational conditions are once again optimal. Fig. 2 (a)-(b) displays the image setting up .

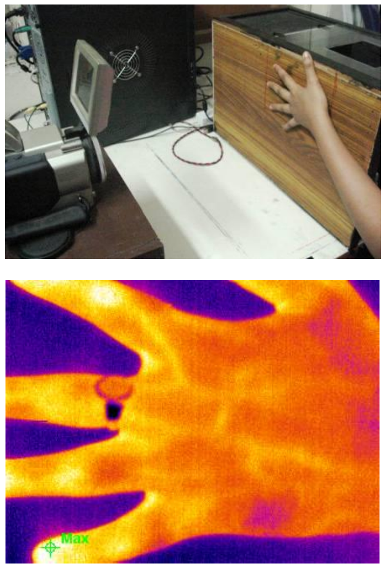

(a)

(b)

Fig. 2 (a) Hand position Setup in front of Camera (b) Captured Image of dorsal vein.

1. These photos are binarized to identify the webbing in between the fingers. The right threshold is selected from the recorded images using a histogram-based binarization technique. Local maxima & the local minimum is determined & identified by analysing the histogram of the dorsa pictures' histogram's bimodal characteristic. This regional minimum serves as the segmentation threshold for the Fig. 3(a) displays the input image and the related histogram (b).

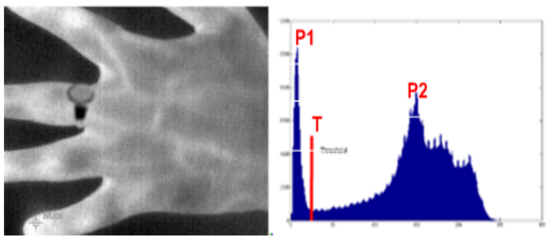

(a) (b)

Fig. 3 (a) Dorsal Vein texture (b) Texture Histogram

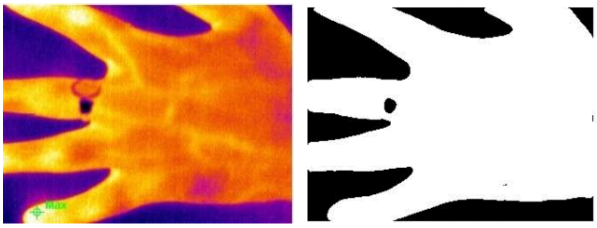

(a) (b)

Fig. 4 (a) Obtained thermal pic (b) Histogram method Binarized Pic

The generalization taking both the standard approach and the graph-based method is shown in Fig. 4(a)-(b).

2. A closed boundary is traced in a clockwise fashion from the binarized image. Once image is binarized boundary points required to be traced , the Jacob's halting criteria are added to the Moore-Neighbour tracing algorithm [22]. The down most left point marked Ps is utilized as the point to start with and the center dot marked Dm is used to calculate the hand's tips and valleys [shown in Fig.5(a)]. Between Wm and the boundary points Ps, we compute their Euclidean distances. As one moves clockwise around the boundary, the distances start to grow until one reaches the tips of the fingers designated as local maxima. Then, when calculated at positions far from the fingertips until local minima are reached. Before beginning to decrease. The middle point between these two points is referred to as the fingertip. Local minimum is located at the valley point. Additionally, as illustrated in Fig. 5, four finger valleys and five tips are identified (b).

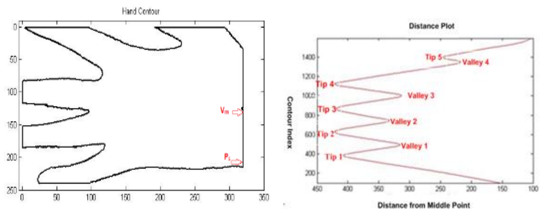

(a) (b)

Fig. 5 (a) Hand contour extracted boundary (b) Obtained hand valleys & Tips

3. Line R1-R2 formed by drawing a tangent between the second and fourth finger valleys. The square region length is determined using corners at R1, R2, R3, and R4 and by a perpendicular distance from the centre point of the line, which has been taken as a reference point. Finally, this square area is clipped and stored as ROI (Fig 6b).

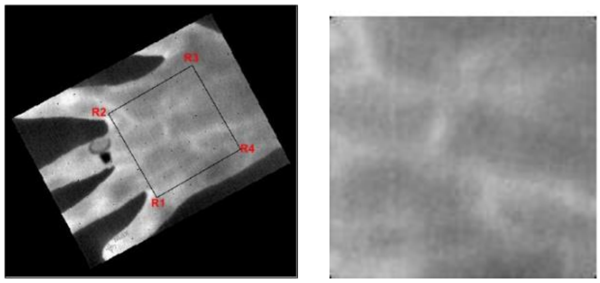

(a) (b)

Fig. 6 (a) Dorsa ROI area (b) ROI Extracted

C. Hand Image aquasation

Using a Canon A630 digital camera, the dorsal portion of the hand is captured. To mount the camera atop it, a wooden box has been taken and a top portion is opened by cutting on its top. A user's hand is supposed to be placed on the box's interior side. Under the box's roof, The focus of camera is set up on hand and the individuals are asked to keep hands in a particular position Fig. 7 displays the imaging setup and the captured images.

(a) (b)

(c)

Fig. 7: The Setup of Camera and dorsal vein samples of acquired

In consideration of achieving reliable and right joined ROI the

3426

Few pre processed steps taken into consideration

1.Binarization 2. segmentation 3. location hand limits (tips and valleys) 4. global hand registration

These steps are briefly explained below:

1. Each collected image is initially binarized by establishing an automated threshold using a histogram-based approach in order to roughly segregate the x dorsum hand region from the images sized. A median filter sized 3x3 can be used to filter out some random noises that are still present because of the uneven illumination. The filtered binary image is then corrected morphologically by removing background fragments using dilatation, filling holes in foreground objects, and reattaching any isolated fingers to the palm that might have been mistakenly binarized due to finger rings as in [14]. The hand dorsum part's resulting binary mask is depicted in Fig. 8. (a)-(c).

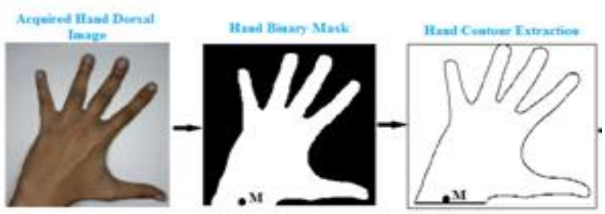

(a) (b) (c)

Fig. 8 (a) acquired Image of hand (b) binarized hand (c) contour of the binarized image.

2. The boundary pixels of the resulting binary mask, which represents the hand's silhouette, are traced and saved as a vector CV (shown in Fig. 8(c)). Finding local minima and maxima points that assist in more exact rotational alignment of the fingers is the main goal of hand contour extraction. Calculating the radial distances between the vector CV & M, the reference point (See Fig. 8 (c)), and storing them in the distance vector DV, is a reliable technique for extracting these contour extremities. This method is comparable to that used in [6], and the distance distribution diagram that is produced is shown in Fig 9.

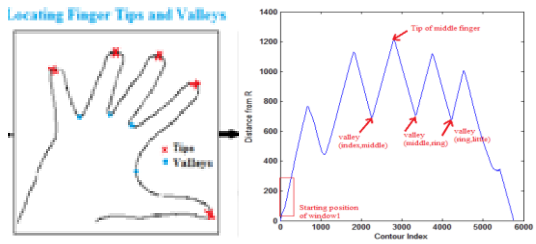

(a) (b)

Fig 9. (a) Locating tips and valleys (b) distance distribution diagram

3. To lower turning variance, each binarized concept passes through all-encompassing hand enrolment however. Worldwide hand registration procedure is the same as that described in [27]. Fig. 10 (a) displays the registered and binarized hand pictures (d).

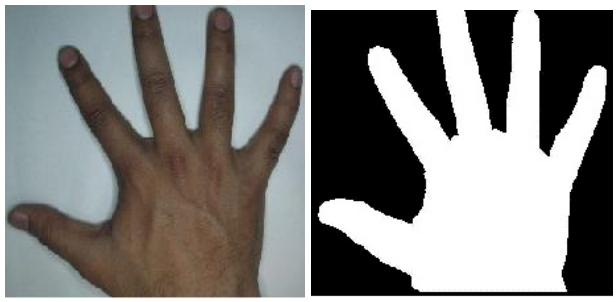

(a) (b)

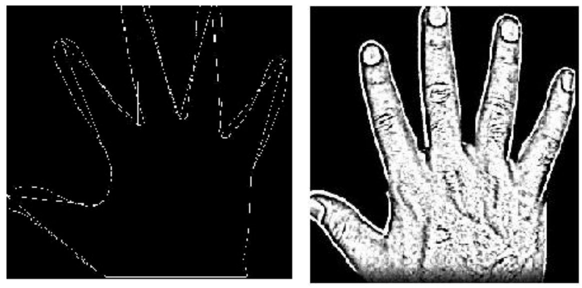

(c) (d)

Fig.10: (a) Indigenous Image (b) binarized Photo (c) registered Photo (d) texturally intensify image

II. Feature Representations of VEIN

A. Vein Characteristic

It have enough information of texture to represent features. The major lines give rise to one type of texture characteristic that can be applied to the matching of two vein images. However, wrinkles—small lines induced by noise acquisition and present in the database's vein patterns—should be distinguished from the primary lines before matching. By recognizing that primary lines have stronger line energy than wrinkles, the separation can be achieved. As a result, the Radon transform is employed to determine the primary lines' orientations and the energy present in the vein patterns.

We can represent straight line in many different ways: by normal representation in polar coordinates, or by the slope-intercept form, k=hx + c in Cartesian coordinates. The angle between y-axis and the line are perpendicular distance from the origin are also given. A line essential along any line in the a-b plane constitutes the transformation of a 2D function [27]. By redefining the Radon transform as follows, Copeland et al. [28] had supported a reduced this transformation:

$$Rad(r,\theta) = \int_{y\min}^{y\max}\int_{x\min}^{x\max} f(x,y)\times(x\cos\theta + y\sin\theta)dxdy \quad (1)$$

A local area is defined by the parameters amax, xmin, ymax, and ymin in [27] to conduct the Radon transform. Moreover, radon-based augmentation has been used in [19] to extract palmprint primary lines and [27] to represent images. The method of Matus et al. [27] makes use of the Radon transform for signals of finite length by adding up the picture pixels along some lines set. The method in[19] modifies [27] using a modulo operation to detect palm lines and lessen the "wrap around" effect. We used [27] for inspiration when implementing the Radon transform for vein patterns. For the real function f [x, y], the work in [27] changed the Radon transform by designating a group Aq =0, 1... q 1, where p is a prime number denoted as:

$$Rad_f(d) = \frac{1}{s}\sum_{(i,j)\in L_d} f(i,j) \quad (2)$$

Here L_d represents a collection of the point that creates a line A2q &e S denotes a scalar that controls the transformed as:

$$L_d = \{(i,j): j = d(i-i_0) + j_0|, i \in Z_p\}, 0 \le d \le q \quad (3)$$

Given (i_0 ,j_0) denotes the middle point of A2q , and d represents the slope of L_d. In this case, Ld stands for a collection of points that were derived from A2q as primary lines, and A2q can be thought of as a local window in the vein ROI. L(), a different notation for Ld that denotes the heading of the line and is derived from:

$$\theta_{d(i_0,j_o)} = arg(\,min_d(\,Rad_f(d))) \quad (4)$$

Energy(i0,j0) = $(min_d(\,Rad_f(d)))$ (5)

For ROI taken for size a×b (Fig. 6 (b)), the middle window A2q (q=17 in our case) travels from pixel to pixel for ROI of size a×b (Fig. 6 (b)). Fig. 11 (b)-(c) display the energy image and the primary line image as a result of applying [Eqn (4) and Eqn. (5)] are shown in Fig. 11 (b)-(c). These photos are combined to produce the improved vein pattern image that gets a match using the normalised Hamming distance by generating matching scores, as seen in Fig. 11(d). 3428

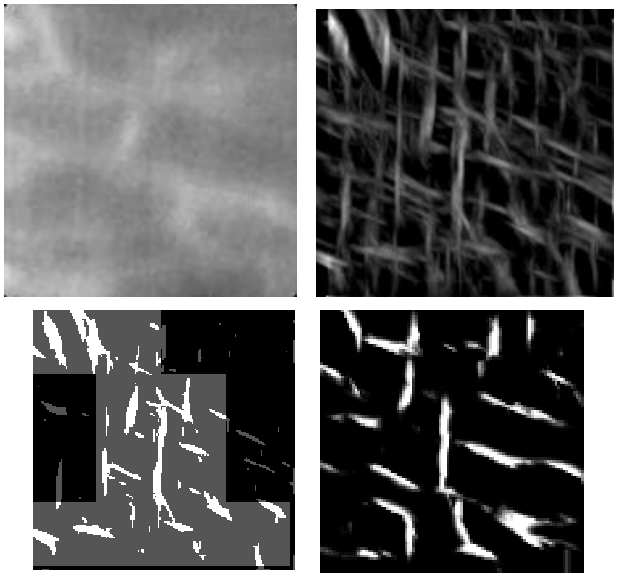

Fig. 11 (a) indigenous ROI (b) Energy (c) principal line(d) The boosted ROI.

A. *Hand Appearance Characteristics*

The hand dorsal part's texture and contour information are available in the normalised and texturally improved hand-appearance images (See Fig. 10(d)), making them the ideal candidates for representation by appearance features derived through the PCA. However, as demonstrated in [24], the independent component analysis (ICA) has been used in hand [20] and face [24] biometrics and is more reliable and well suited for extracting appearance traits. In this study, hand appearance photos are used to extract appearance features using ICA, which breaks down a mixed signal into additive non-Gaussian subcomponents [26] To get ICA features, the relationships in the hand-shape images must be broken out into separate elements. In [26], ICA's theory and application are addressed. Now, these feature specifics are in order.

A hand-appearance image is viewed by the ICA modeled as concatenation of (ICs) & a merging matrix. Let us X_{KxN} represent the hand-appearance image, M_{NxN} represent the mixing matrix, and C_{KxN} represent the ICs matrix:

$$X_{D\times B} = C_{D\times B} \times M_{B\times B} \quad (6)$$

Estimating the free elements from the source images is the task in ICA:

$$S = X \times (A^{-1}) \quad (7)$$

Blind Source Separation is the phrase used here to describe the process of deriving S from X because, without knowing the mixing matrix, it is necessary to divide the input source into independent components. We employed the FastICA algorithm [26], which uses negentropy maximization to maximize notwithstanding the fact that the output elements' statistical independence that there are numerous methods for estimating ICs from Eqn (6).

Here, we've employed a database of 200 people, each with five examples of their hand appearance. Each hand-shaped image is 200 by 200 pixels in size. The average of the five enrolled samples photos is used to calculate the average sample picture for every user. To produce a vector graphic with a scale of n40000x1, the average of sample image taken is scaled. All users' addressed (150) ,mean-sample images are calculated using the picture matrix $X_{40000x200}$, where D=40000 and B=200. PCA is used to reduce the dimensionality of X because it is discovered to have a high number of dimensions. Let $Mean_{40000x1}$ be the mean vector which we have obtained from the application of PCA on, and let $U_{40000x200}$ be the projection (eigenvector) matrix. The projection matrix $Y_{200x200}$ is created via PCA after the image matrix X has been processed.as follows:

$$Y_{200\times200} = (X_{40000\times200})^{T} \times U_{40000\times200} \quad (8)$$

Expressions (6) and (7) are used to derive the IC matrix, $S_{200x200}$, from the projecting matrix Y after executing the Fast ICA method (7). Let $Q_{40000x1}$ be the imaging matrices calculated from the input gestures at the validation/ identification phases. It results when the mean vector $Mean_{40000x1}$ is subtracted from it

$$Vector1_{40000\times1} = (Q_{40000\times1}) - (\,Mean_{40000\times1}) \quad (9)$$

The Eigen feature set is produced by multiplying Vector1 by the PCA projection matrix as:

$$Eigenfeature_{1\times200} = Vector1_{40000\times1}{}^{T} \times U_{40000\times200} \quad (10)$$

The ICA characteristic vector is produced by applying the IC matrix to the Eigen feature vector: 3429

$$ICAfeature_{200\times1} = B_{200\times200} \times Eigenfeature_{1\times200}{}^{T} \quad (11)$$

Here, two ICA feature vectors are matched using the Euclidean distance. Using Eq.(11), compute the two ICA features ICAV1 and ICAV2. These 2 vectors' matching score $\mathbf{S_1}$calculated as:

$$S1 = \sqrt{\sum_{i=1}^{150}\{\boldsymbol{ICAV_1(i) - ICAV_2(i)}\}^2} \quad (12)$$

III EXPERIMENTAL RESULTS

Five samples has been collected from a 200 user’s database. Each user’s sample has been committed in db then the ICA features for dorsal hand forms and the Radon features for vein patterns are retrieved. Three samples are picked from the five enrolled images for training, while for testing we used the remaining other samples. Each user's few training & testing samples has been collected and compared using the Euclidean distance, then all the scores which matched during this has been taken. Authentic score will be calculated if the scores are getting match of both (train & test), if train & test didn’t matched we refer it as imposter one(imposter score). So, to calculate all 3 matched scores in the case of a real matching score, all three training photos of a claimed identity for authentication are matched to the 1st test subject of the claimed user. Of this lowest of these scores is considered to be the true result from the first test sample. A similar matching score is produced for the same user for a different test image. As a result, 400 real matching scores (200x2) are computed for 200 users across both hand and vein patterns. The (199x2) test images of an additional 398 people are matched with all three of a user's train images to determine the impostor matching score. The imposter score related to each test user is kept as the lowest of the three matches. As a result, for 200 users, 79600 (200x199x2) computations for both hand forms and vein patterns are made.

1. *The scores Matched*: All matched scores are determined by matching the testing samples and training samples of each claimed identity influenced with Euclidean distance. All matching scores are known as the authentic score, otherwise, impostor scores, if the training & testing samples (image) come from the one person. Therefore, to compute three matching scores in the case of true matched scores, entire three training photos of a user are matched with the user's primary samples taken (3). Of these lowest of these scores is considered to be the true result from the first test sample. The identical user also receives a matching score on a different test image. As a result, 300 real matching scores (150x2) are computed for 150 users across both hand and vein patterns. The (149x2) test images of an additional 149 individuals are matched with all three of a user's train images to determine the impostor matching score. Each test user's impostor score is kept as long as there are at least three matches. Therefore, 44700 (150x149x2) are calculated for 150 users for both the dorsal vein traits & its shapes.

2. *The Errored Rate:* Errored Rate are determined by matching real and fake scores to a threshold. False rejection rate (FRR) is the proportion of genuine matching scores that are not accepted by the decision-threshold, whereas false acceptance rate (FAR) is the proportion of fake scores that are not rejected (FAR). The minimal FAR must be provided for a typical biometric authentication in order to obtain the associated genuine acceptance rate calculated by GAR = 100 – FRR.

3. ROC: Threshold was adjusted to plot the curve on FAR vs. GAR and then the value for FARs and GARs has been calculated. Traditional biometric systems consider, the ROC is used to choose threshold that produces the lowest FAR. During the verification stage, decisions about acceptance and rejection are made using this criterion. The shape of the hand and the veins in the hand serve as excellent biometric indicators, as seen by this curve.

The graphs and modalities of matching scores & ROC of the dorsal shape & veins are presented in Fig. 12 (a)-(c).

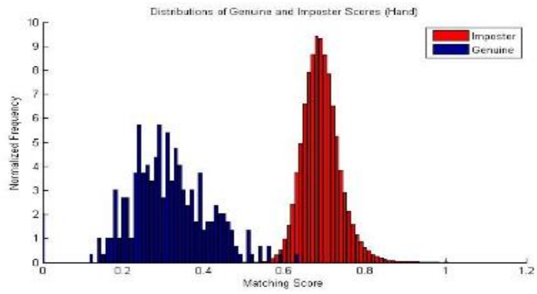

(a)

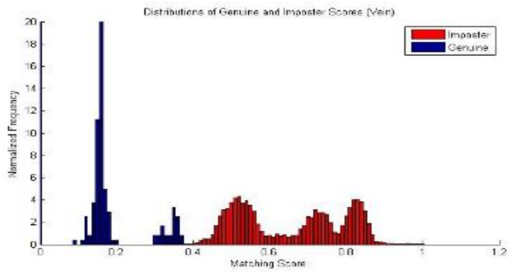

(b)

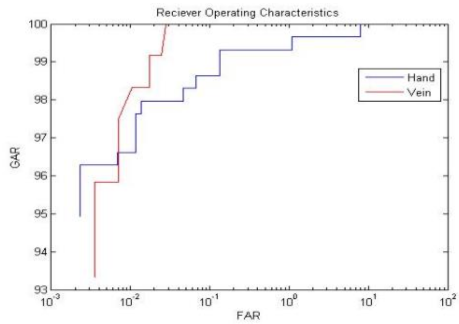

(c)

Fig. 12: Histogram Distribution of matching scores on hand-shape: (a) hand-shape (b) Hand-vein patterns Distribution of histogram for the matching scores; (c) Combined ROC for above plots.

It can be observed from 12 (c) that, with minimum FAR, hand dorsa is operating on better accuracy. However, with a little bit increase in FAR, hand vein provides better accuracy than hand dorsa.

A. Score level Fusion

By comparing each user to other enrolled users, the score matrices from each biometric matcher can be produced. The computed score is referred to as a legitimate score if samples from the same user are matched, and an imposter score otherwise. It is necessary to normalise the matching scores calculated from B biometric matchers because they may have a wide range [21]. In this study, the matching score matrix was normalised using the min-max method. The min-max normalisation can be expressed as follows, assuming that MScore is the matching score matrix obtained from a biometric matcher:

$$M_{Score} = \frac{M_{Score} - Min(M_{Score})}{Max(M_{Score})} \quad (13)$$

Numerous fusion at score level fusion rules have been put out in the literature for multimodal any level of biometric verification [21 and 25]. However, the majority of them are linear fusion rules, including the min, sum, product, and max rules. In a recent study, Kumar et al. [24] suggested non-linear fusion rules like tanh and *exp* and shown promising results in their modified adaptive fusion framework. Four score-level fusion rules are taken into consideration in this study for the fusion of the matching score matrices from biometric matchers: sum, product and other rules When j=1 to B for B modalities, W_j should be the corresponding weight for the matching score matrices. The matching matrices' fusion rules can be summed up as follows::

$$Sum = \sum_{j=1}^{B} W_j \times M_{Score}^{j} \quad (14)$$

$$\text{Product} = \prod_{j=1}^{B} \left(M_{Score}^{j}\right)^{W_j} \quad (15)$$

$$exp = \sum_{j=1}^{B} exp(M_{Score}^{j}) \times W_j \quad (16)$$

$$tanh = \sum_{j=1}^{B} tanh(M_{Score}^{j}) \times W_j \quad (17)$$

The ROC curve in multimodal hand vein fusion with hand dorsa using the fusion rules defined above is given in Fig 13.

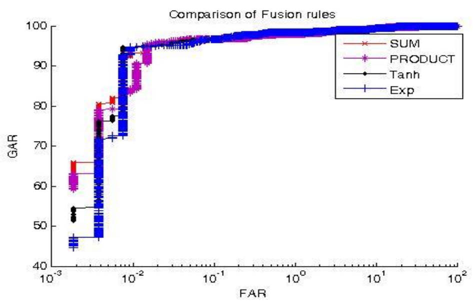

Fig 13: GAR Vs FAR

From it has be observed that for minimum FAR (0.001%) Product rule worked on high accuracy (80%). However, with slight increase in FAR (0.01%) SUM rule provides better accuracy (98%).

IV Conclusion

Dorsal hand veins and visual hand dorsa features (Shape + Appearance) are used in this paper to create a novel bimodal system. The user's hands can concurrently extract both attributes, and the claimed identification is verified by fusing them together using four fusion rules (Section IV C). The experimental results taken on 200 users features explains that the inbuilt vein pattern building, which contains virtues like individuality, reliability, and strong exemption against falsification as well as the exterior hand dorsal structure, which provides an effective appearance feature, have the prospects to reliably authenticate the proposed bimodal system. Due to its ability to record both internal and external structural information, our multimodal system is distinctive. We intended to employ an adaptive security mechanism in the suggested multimodal system in subsequent work so that it could adapt to different security settings.

References

[1] D. Maltoni, D. Maio, A. K. Jain, S. Prabhakar, Eds., Handbook of Fingerprint Recognition, Springer, 1st edition, 2003.

[2] B. S. Atal, "Automatic Recognition of Speakers from Voices", Proc. IEEE, Vol. 64, pp. 460-475, 1976.

[3] T. Kanade, "Picture Processing System by Computer Complex and Recognition of Human Faces", PhD Thesis, Department of Information Science, Koyoto University, 1973.

[4] R. Nagel and A. Rosenfeld, "Computer Detection of Freehand Forgeries", IEEE Transaction on Computers, Vol. 26(9), pp. 895-905, 1977.

[5] A. Jain, R. Bolle, and S. Pankanti, Biometrics-Personal Identification in a Networked Society, Norwell, Kluwer, 1999.

[6] N. Ratha and R. Bolle, Eds., Automatic Fingerprint Recognition Systems, Springer, October, 2004.

[7] J. Wayman, A. K. Jain, D. Maltoni, and D. Maio, Eds., *Biometric Systems: Technology, Design, and Performance Evaluation*, Springer, 2005.

[8] A.K. Jain and N.K. Ratha, Eds., Proc. SPIE, *Biometric Technology for Human Identification* I, Vol. 5404, 2004.

[9] J. Kittler and M. S. Nixon, Eds., Fourth International Conference on Audio- and Vedio-Based Biometric Person Authentication, Vol. 2688, LNCS, Springer, 2003.

[10] BioSec, Biometrics and Security, FP6 IP IST - 2002-001766, 2004, Available at: http://www.biosec.org/.

[11] A.Kumar, H Hanumandu"Biometric authentication based on infrared thermal hand vein patterns" IEEE, Dec 2009.

[12] A.Kumar, M Hanmandlu"Fuzzy binary decision tree for biometric based personal authentication" Elsevier 2013

[13] A.Kumar, Madasu Hanmandlu, HM Gupta "Ant colony optimization based fuzzy binary decision tree for bimodal hand knuckle verification system" Pergamon 2013

[14] BioAPI, ANSI INCITS, 358-2002-Information Technology- BioAPI Specification, 2002 (Version 1.1).

[15] P. J. Phillips, H. Moon, P. J. Rauss, and S. Rizvi, "The FERET Evaluation Methodology for Face Recognition Algorithms", IEEE Transaction on Pattern Analysis and Machine Intelligence, Vol. 22(10), pp. 1090-1104, 2000.

[16] M. Przybocki, and A. Martin, "NIST Speaker Recognition Evaluation Chronicles", ISCA Workshop on Speaker and Language Recognition, ODYSSEY, pp. 15-22, Spain, 2004.

[17] A.Kumar, A.Kumar" Online biometric authentication using hand vein patterns" IEEE Symposium on Computational Intelligence for Security and Defense 2009 Journal.

[18] E. S. Bigun, J. Bigun, B. Duc, S. Fischer, "Expert conciliation for multi modal person authentication systems by Bayesian statistics", Proc. IAPR International Conference on Audio-and Video-based Person Authentication (AVBPA), Springer, Vol. 1206, pp. 291-300, 1997.

[19] L. Hong, A. K. Jain, "Integrating Faces and Fingerprints for Personal Identification", IEEE Transaction on Pattern Analysis and Machine Intelligence, Vol. 20 (12), pp. 1295-1307, 1998.

[20] K. Nandkumar, "Integration of Multiple Cues in Biometric Systems", MS Thesis, Deaprtment of Computer Science and Engineering, Michigan State University, 2005.

[21] A. Kumar, "Rank level fusion," in Encyclopedia of Biometrics, S.Li, (Ed.) New York: Springer Verlag, 2009.

[22] K. Veeramachaneni, L. A. Osadciw, and P. K. Varshney, "An Adaptive Multimodal Biometric Management Algorithm", IEEE Transaction on Systems, Man, and Cybernetics—Part C: Applications and Reviews, Vol. 35(3), August, 2005.

[23] A. Kumar, V. Kanhangad, and D. Zhang, "A New Framework for Adaptive Multimodal Biometrics Management", IEEE Trans. on Information Forensics and Security, Vol. 5(1), pp. 92-102, March, 2010.

[24] J. Kittler, M. Hatef, R. P. W. Duin, and J. Matas, "On combining classifiers", IEEE Transaction on Pattern Analysis and Machine Intelligence, Vol. 20(3), pp. 226–239, March 1998.

[25] K. Nandakumar, Y. Chen, S. C. Dass, and A. K. Jain, "Likelihood Ratio Based Biometric Score Fusion", IEEE Transaction on PAMI, Vol. 30(2), pp. 342-347, 2008.

[26] F. Matus, J. Flusser, "Image Representations via a Finite Radon Transform", *IEEE Transactions on Pattern Analysis and Machine Intelligence*, Vol. 15(10), pp. 996–1006, 1993.

[27] A.C. Copeland, G. Ravichandran, M.M. Trivedi, Localized radon transform-based detection of ship wakes in SAR images, IEEE Transaction on Geo-science Remote Sensing, Vol. 33 (1), pp. 35–45, 1995.

.